Tsinghua Science and Technology

Volume 23 | Issue 6 Article 8

2018

A Robust Graph Optimization Realization of Tightly Coupled GNSS/INS Integrated Navigation System for Urban Vehicles

Wei Li
the Department of Electronic Engineering, Tsinghua University, Beijing 100084, China.

Xiaowei Cui
the Department of Electronic Engineering, Tsinghua University, Beijing 100084, China.

Mingquan Lu
the Department of Electronic Engineering, Tsinghua University, Beijing 100084, China.

TSINGHUA SCIENCE AND TECHNOLOGY
ISSN 1007-0214 08/10 pp 724–732
DOI: 10.26599 / TST.2018.9010078
Volume 23, Number 6, December 2018

A Robust Graph Optimization Realization of Tightly Coupled GNSS/INS Integrated Navigation System for Urban Vehicles

Wei Li, Xiaowei Cui*, and Mingquan Lu

Abstract: This paper describes a robust integrated positioning method to provide ground vehicles in urban environments with accurate and reliable localization results. The localization problem is formulated as a maximum a posteriori probability estimation and solved using graph optimization instead of Bayesian filter. Graph optimization exploits the inherent sparsity of the observation process to satisfy the real-time requirement and only updates the incremental portion of the variables with each new incoming measurement. Unlike the Extended Kalman Filter (EKF) in a typical tightly coupled Global Navigation Satellite System/Inertial Navigation System (GNSS/INS) integrated system, optimization iterates the solution for the entire trajectory. Thus, previous INS measurements may provide redundant motion constraints for satellite fault detection. With the help of data redundancy, we add a new variable that presents reliability of GNSS measurement to the original state vector for adjusting the weight of corresponding pseudorange residual and exclude faulty measurements. The proposed method is demonstrated on datasets with artificial noise, simulating a moving vehicle equipped with GNSS receiver and inertial measurement unit. Compared with the solutions obtained by the EKF with innovation filtering, the new reliability factor can indicate the satellite faults effectively and provide successful positioning despite contaminated observations.

Key words: Global Navigation Satellite System (GNSS); sensor fusion; Inertial Navigation System (INS); optimization; factor graph; tightly coupled integration

1 Introduction

Ground vehicles that aim to fulfill specific tasks such as route planning and self-driving rely on the accurate localization results mainly provided by the Global Navigation Satellite System (GNSS). However, GNSS signals are susceptible to artificial interference or other negative effects, such as non-line-of-sight, multipath, and attenuation. These effects will provoke deterioration of GNSS' positioning accuracy, so identifying contaminated measurements and obtaining a reliable solution are important, especially for safety critical applications. To enhance the performance of standalone GNSS in urban settings, receivers can be augmented with other sensors and barometric altimeters[1, 2], Inertial Navigation Systems (INSs)[3] and vision systems[4] have all been considered. Among the above sensors, the combination of INS and GNSS is most widely applied because of their complementary properties. Accurate positioning results obtained from GNSS can correct errors accumulated over time in INS. Although INS measurements are immune to external interference, they can supply the integrated navigation system with high-rate velocity and attitude and provide a short-term positioning solution by dead reckoning when GNSS is absent. GNSS/INS integrated navigation systems are typically classified as loosely, tightly, and ultra-tightly coupled architectures[5]. In loosely coupled techniques, GNSS and INS provide the position

• Wei Li, Xiaowei Cui, and Mingquan Lu are with the Department of Electronic Engineering, Tsinghua University, Beijing 100084, China. E-mail: wli14@mails.tsinghua.edu.cn; cxw2005@mail.tsinghua.edu.cn; lumq@mail.tsinghua.edu.cn.

* To whom correspondence should be addressed.
Manuscript received: 2017-12-19; accepted: 2018-01-18

and velocity results, respectively. When the number of visible satellites is insufficient, the techniques fail. In the case of ultra-tightly coupled method, INS and integration Kalman filter work as parts of a loop filter of a generic GNSS receiver; this technique belongs to the field of receiver design and is difficult to implement in software. A deep degree of coupling leads to improved navigation performance. Considering the shortcomings of the abovementioned integrated navigation systems, the tightly coupled GNSS/INS system is currently the most widely used integration architecture. The main benefit of tight integration is enhanced system availability, which permits positioning results to be obtained in scenarios with poor signal quality or limited coverage[6].

The typical tightly coupled integration structure is realized by merging GNSS raw measurements (i.e., pseudorange and Doppler observables) and INS navigation solutions through a Bayesian filter. The positioning issue is viewed as a non-linear estimation problem and typically solved by the Kalman filter and its extended variants[7], including the unscented Kalman filter[8] and iterated Extended Kalman Filter (EKF). From a mathematical perspective, existing filtering methods have two major disadvantages. First, they show instability when solving nonlinear estimation problems. The EKF, for instance, only evaluates the Jacobians once at a single time step by using Markov assumption to achieve its recursive form. The lack of iteration may not yield a convergent result when the system is nonlinear[9], and it fails to take full advantage of previous information. Second, the filtering methods are sensitive to faulty measurements. The operating point of linearization in EKF is the mean of previous estimations, and it may be deviated from the true state because of defective observations. Improper operating points will lead to bad linearization of the positioning process, causing bias and inconsistency under complicated environments.

To avoid the first defect of existing filtering algorithms, the optimization methods are used to solve non-linear localization in the field of robotics. The batch optimization algorithms can iterate over the whole trajectory and converge to a better operating point. However, iteration brings a large amount of computations that are considered post-processing[7]. Thus, batch optimization methods have rarely been applied to tightly coupled GNSS/INS integration systems. Circumstances have changed in recent years, and researchers in robotics have found two ways to perform optimization in real-time. The first approach is to solve the optimization problem under a sliding window framework. The main perspective of the approach is to avoid infinite growth of iteration time by limiting the size of the state vector. The sliding window algorithm can scale from exhaustive batch solutions to fast incremental solutions by tuning several parameters[10]. The second approach is to reduce the computation of optimization iteration by exploiting the sparse connectivity of the observation process[11]. The factor graph is introduced[12] to identify the part that needs to be updated, and it is used to solve Simultaneous Localization And Mapping (SLAM) issues[13]. Furthermore, a factor graph can be transformed into a Bayes net[14]. Using the property of chordal Bayes net, Cholesky decomposition in the gradient descent algorithm can be simplified effectively, and the iteration time is shortened.

To avoid the second defect of existing filtering algorithms, faulty measurements should be distinguished from good ones. To detect incorrect GNSS measurements and exclude them, a concept named Receiver Autonomous Integrity Monitoring (RAIM) was introduced in 1987. Most existing implementations of RAIM algorithms utilize GNSS-only measurements to assess consistency, with an assumption of single satellite failure[15, 16]. This assumption is not applicable in degraded signal environments confronted by urban vehicles, because the obstacles may cause more than one signal error simultaneously. Although more than one outlier is available, the classic RAIM algorithms are unable to distinguish the wrong measurements and isolate them. To solve this problem, some probabilistic algorithms can be adopted as the pretreatment processes. In the existing implementation of a tightly coupled GNSS/INS system, innovation filtering is a common feature of Kalman filter designs[17], especially for applications with integrity requirements. Innovation filtering sets a threshold and rejects the measurement whose normalized innovation exceeds the threshold, so that it can filter out violent changes. However, innovation filtering performs poorly when measurement errors grow, because the state estimates are contaminated by errors in each iterate step.

In this paper, we propose a tightly coupled GNSS/INS integrated positioning algorithm based on graph optimization, which is factored with robust adaptation and real-time performance. There are some obvious differences in the choice of state variables and graph presentation between this paper and the previous literature[18, 19]. To obtain accurate motion estimations, we add the accelerometer and gyro biases to state variables, and the structure of the factor graph is changed

accordingly. In addition, our algorithm records the entire trajectory, so the preceding GNSS measurements and motion constraints between adjacent GNSS epochs can provide redundant information for outlier elimination. Inspired by the concept of switchable constraints[20] in the domain of SLAM, we construct a robust cost function by introducing a new reliability factor in the original state variables, so that the new factor can indicate which satellite measurement is contaminated while positioning in process. Furthermore, our algorithm complies with the requirements of real-time applications by exploiting the sparse connectivity of observations through the factor graph.

This paper is organized as follows. We first provide a brief review of related work in Section 1. Section 2 uses Bayes' rule to express the integrated navigation problem as a product over several error functions. Section 3 shows how the vehicle states and sensor observations can be modeled as a factor graph. Section 4 provides the algorithm to solve incremental optimization from a Bayesian inference perspective. Section 5 presents an evaluation of the proposed method on simulated datasets. The last section discusses the conclusion and future work.

2 MAP Estimation in Integrated Navigation

The goal of all types of localization methods is to find the most likely posterior state given the measurements from sensors. Thus, the positioning problem can be formulated as a Maximum A Posteriori (MAP) problem,

$$\hat{\boldsymbol{x}}=\arg\max_{\boldsymbol{x}} P(\boldsymbol{x}_{0:t}\,|\boldsymbol{z}_{0:t},\boldsymbol{u}_{0:t}) \tag{1}$$

where $\hat{\boldsymbol{x}}$ presents the optimal estimation for the state variables of the system, $\boldsymbol{z}_{0:t}$ presents all the GNSS observations from the beginning. Moreover, $\boldsymbol{u}_{0:t}$ presents all the prior information, which is equivalent to motion information from INS. Given that GNSS measurements and INS information are independent of each other, Bayes' rule[9] allows us to factor the expression above as

$$\hat{\boldsymbol{x}}=\arg\max_{\boldsymbol{x}} \prod_{t,j} P(z_{t,j}\,|x_t)\prod_{t} P(x_t\,|x_{t-1},u_t) \tag{2}$$

where $z_{t,j}$ is the measurement from the j-th satellite at a fixed time t. Thus, MAP estimation is expressed as a product over several single factors. By constructing appropriate error functions, the whole problem can be modeled as a factor graph, and Bayesian inference is used to obtain the optimal solution.

3 Factor Graph Formulation

Factor graph was proposed by Kschischang et al.[12] to model factorizations. Formally a factor graph is a bipartite undirected graph, including vertexes and edges: vertex θ_i presents the state variable of different moments, and the edge connecting two vertexes presents the error function $e_{ij}(\cdot)$; each edge corresponds to a single observation $z_{i,j}$. When a new observation arrives, only nodes associated with the current observation need to be updated.

Figure 1 shows an example of the factor graph formulation in a previous study[11], where IMU means Inertial Measurement Unit. In this figure, INS and GNSS operate at different frequencies, and there is a lack of modeling for biases of inertial sensors.

According to Eq. (2), we use f to define the probability distribution of state variables. Thus, the whole factor graph defines factorization as

$$f(\boldsymbol{\Theta})=\prod_i f_i(\theta_i) \tag{3}$$

Through comparison with MAP problem, the goal of the graphical model is

$$\hat{\boldsymbol{\Theta}}=\arg\max_{\boldsymbol{\Theta}} \prod_i f_i(\theta_i) \tag{4}$$

When the observation noises accord with Gaussian distribution, the negative logarithm of probability distribution is proportional to the error function, and the MAP estimation can be converted to a non-linear least squares problem:

$$\hat{\boldsymbol{x}}=\arg\min_{\boldsymbol{x}} \sum_{i,j} e(x_i,x_j,z_{i,j})^{\mathrm{T}}\boldsymbol{\Omega}_{i,j}{}^{-1}e(x_i,x_j,z_{i,j}) \tag{5}$$

where $\boldsymbol{\Omega}_{i,j}$ represents the information matrix of a constraint relating the parameters x_i and x_j, and it decides the weight of an error function over the entire optimization problem. $e_{ij}(\cdot)$, as the abbreviation of $e(x_i,x_j,z_{i,j})$, presents a residual function for all the observations available from both GNSS receiver and inertial measurement unit.

Although the positioning problem solved by the optimization method will be formulated as an objective

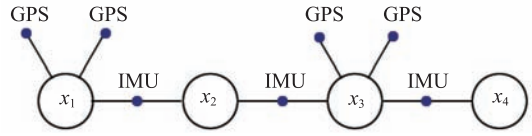

Fig. 1 Graph structure in Ref. [11].

function, which needs to be optimized, the selection of state variables and error functions may influence algorithm performance. Figure 2 illustrates the factor structure of our optimization algorithm. The large nodes represent state variables. There are three types of state variables: vehicle state $\boldsymbol{x}_{\text{veh}}$, satellite state $\boldsymbol{s}$, and inertial unit state $\boldsymbol{x}_{\text{ine}}$. Small nodes on the edges represent the error functions corresponding to different measurements. The specific implementation will be explained in the following subsections.

3.1 Motion model constraint

The blue node in Fig. 2 between two vehicle states represents the velocity error function. The vehicle state in this paper is connected to the edges of pseudo-range (pseudo-range rate) and INS measurements. It contains the 3D position and velocity of the vehicle, as well as the clock error relative to satellite and its drift.

$$\boldsymbol{x}_{\text{veh}} \in \mathbb{R}^8 = (r_1, r_2, r_3, v_1, v_2, v_3, \delta^{\text{clock}}, \dot{\delta}^{\text{clock}}) \tag{6}$$

Given that GNSS observations do not update the attitude, the vehicle state here does not contain Euler angles. With the aid of odometry information, we use a constant velocity model to constrain the changes in both position $\boldsymbol{r}^t = (r_1^t, r_2^t, r_3^t)$ and clock error. The error function is

$$\boldsymbol{e}_{\text{vel}}^t = \begin{pmatrix} r_1^{t+1} \\ r_2^{t+1} \\ r_3^{t+1} \\ \delta_{t+1}^{\text{clock}} \\ \dot{\delta}_{t+1}^{\text{clock}} \end{pmatrix} - \begin{pmatrix} r_1^t + (v_1^t + v_1^{t+1}) \cdot \Delta t/2 \\ r_2^t + (v_2^t + v_2^{t+1}) \cdot \Delta t/2 \\ r_3^t + (v_3^t + v_3^{t+1}) \cdot \Delta t/2 \\ \delta_t^{\text{clock}} + \dot{\delta}_t^{\text{clock}} \cdot \Delta t \\ \dot{\delta}_t^{\text{clock}} \end{pmatrix} \tag{7}$$

With $\boldsymbol{\Omega}_{\text{vel}}^t = \text{diag}(\sigma_t^1, \sigma_t^2, \sigma_t^3, \sigma_t^{\text{clock}}, \sigma_t^{\text{clockdrift}})$ is the covariance matrix associated with the vehicle state factor.

3.2 Inertial sensor's constraint

The red node in Fig. 2 between a vehicle state and an inertial unit state represents the inertial error function. The selection of an inertial unit state depends on the sensor we use. This paper considers a single integration of gyro and accelerometer; thus, the inertial measurements include attitude $\boldsymbol{\omega}_{ib}^b$ and specific force $\boldsymbol{f}^b$. The gyro measurement model[7] is

$$\boldsymbol{m}_{\text{gyro}} = \boldsymbol{\omega}_{ib}^b + \boldsymbol{y}_g + \boldsymbol{\nu}_g \tag{8}$$

where $\boldsymbol{\nu}_g$ is Gaussian white noise, and $\boldsymbol{y}_g$ is a bias modeled as a first-order Gauss-Markov process. Similarly, the accelerometer measurement model is

$$\boldsymbol{m}_{\text{accel}} = \boldsymbol{a}_{ib}^b + \boldsymbol{g}^b + \boldsymbol{y}_a + \boldsymbol{\nu}_a \tag{9}$$

where $\boldsymbol{\nu}_a$ is Gaussian white noise, and $\boldsymbol{y}_a$ is a random walk bias. The acceleration and angular velocity are obtained according to the kinematic equations, and Euler angles (θ, ϕ, ψ) are transformed from the direction cosine matrix $\boldsymbol{R}_b^e$. For instance, in the ECEF frame:

$$\dot{\boldsymbol{v}}^e = \boldsymbol{R}_b^e \boldsymbol{f}^b + \boldsymbol{g}^e - 2\boldsymbol{\Omega}_{ie}^e \boldsymbol{v}^e \tag{10a}$$

$$\dot{\boldsymbol{R}}_b^e = \boldsymbol{R}_b^e (\boldsymbol{\Omega}_{ib}^b - \boldsymbol{\Omega}_{ie}^b) \tag{10b}$$

To increase the accuracy of motion estimation, we add the calibration parameters $\boldsymbol{y}_g$ and $\boldsymbol{y}_a$ to the inertial unit state. These parameters make our graph structure different from those in Ref. [19]. The inertial constraint edge connects an inertial unit state vertex and a vehicle state vertex. Velocity and attitude will be updated when a new INS observation comes. The velocity vector belongs to the vehicle state; thus, the remaining Euler angles belong to the inertial unit state.

$$\boldsymbol{x}_{\text{ine}} \in \mathbb{R}^9 = (\theta, \phi, \psi, \boldsymbol{y}_g, \boldsymbol{y}_a) \tag{11}$$

Accordingly, the error function of inertial constraint is

$$\boldsymbol{e}_{\text{ins}}^t = \begin{pmatrix} v_1^{t+1} \\ v_2^{t+1} \\ v_3^{t+1} \\ \theta_{t+1} \\ \phi_{t+1} \\ \psi_{t+1} \\ \boldsymbol{y}_g^{t+1} \\ \boldsymbol{y}_a^{t+1} \end{pmatrix} - \begin{pmatrix} v_1^t + \dot{v}_1^t \cdot \Delta t \\ v_2^t + \dot{v}_2^t \cdot \Delta t \\ v_3^t + \dot{v}_3^t \cdot \Delta t \\ \theta_t + \dot{\theta}_t \cdot \Delta t \\ \phi_t + \dot{\phi}_t \cdot \Delta t \\ \psi_t + \dot{\psi}_t \cdot \Delta t \\ \boldsymbol{y}_g^t \\ \boldsymbol{y}_a^t \end{pmatrix} \tag{12}$$

3.3 Switchable pseudorange constraint

The green node in Fig. 2 between a vehicle state and a satellite state represents the GNSS error function. Each observation of a satellite provides a pseudorange measurement ρ_{tj}, and a pseudorange rate measurement $\delta\rho_{tj}$, with the prior knowledge of satellite position. The measurement function[21] is

$$\boldsymbol{m}_{\text{GNSS}}^t = \begin{bmatrix} m_{\text{pr}}^t \\ m_{\text{prr}}^t \end{bmatrix} = \begin{bmatrix} \left\| \boldsymbol{p}_{t,j}^{\text{SAT}} - \boldsymbol{p}_t \right\| \\ \left\| \boldsymbol{v}_{t,j}^{\text{SAT}} - \boldsymbol{v}_t \right\| \end{bmatrix} +$$

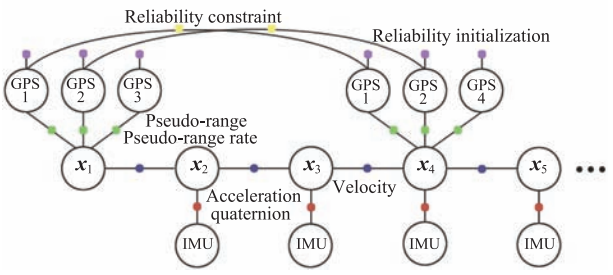

Fig. 2 Graph structure in this paper.

$$\begin{bmatrix} \delta^{\mathrm{ER}}+\delta^{\mathrm{RE}}+\delta^{\mathrm{AT}}+c\cdot\delta_t^{\mathrm{clock}} \\ \dot{\delta}^{\mathrm{ER}}+c\cdot\dot{\delta}_t^{\mathrm{clock}} \end{bmatrix} \tag{13}$$

where δ^{ER}, δ^{RE}, and δ^{AT} present the effects to position caused by earth's rotation, relativity, and atmosphere, respectively. Considering the satellite measurements may have potential fault, a new reliability factor is introduced to enhance the system's robustness. The only variable of satellite state is the reliability factor $s_{t,j}$. We construct a continuous function $w(s_{t,j})$ as a weighted value of the GNSS measurement. If we consider both pseudorange and its rate, the reliability factor will be expanded into a 2D one.

$$\boldsymbol{s}\in\mathbb{R}^2=\left(s_{t,j}^1,s_{t,j}^2\right) \tag{14}$$

Thus the pseudorange error function is

$$\boldsymbol{e}_{\mathrm{GNSS}}^t=\begin{pmatrix} w(s_{t,j}^1)\cdot(m_{\mathrm{pr}}^t-\rho_{tj}) \\ w(s_{t,j}^2)\cdot(m_{\mathrm{prr}}^t-\delta\rho_{tj}) \end{pmatrix} \tag{15}$$

We define $w(s_{t,j})\in[0,1]$. When the value of $w(s_{t,j})$ is closed to zero, the satellite measurement is regarded as an outlier. In the topological interpretation, the reliability factor is set to zero to make an edge "invisible". Thus, it is also a convenient way to convert the full trajectory optimization to partial optimization.

The yellow node in Fig. 2 between two states from the same satellite at adjoining moments represents the reliability error function. Considering the stability of the satellite's observability, the error function is used as a constraint to ensure the reliability factors of the same satellite will not change rapidly. Therefore, the corresponding function is

$$\boldsymbol{e}_{\mathrm{rel}}^t=\boldsymbol{s}_{t+1,j}-\boldsymbol{s}_{t,j} \tag{16}$$

If the goal is to minimize the sum of error functions, then setting all reliability factors to zero will reach numerical satisfaction. However, this condition is not expected to find the successful position, so we need a constant initial value $\boldsymbol{\gamma}_j$ as anchors to the reliability factors. The constraint between fixed value and reliability factor is illustrated in Fig. 2 as the purple node. The edges exist to prevent the optimization process to reject all measurements. The error function is then defined as

$$\boldsymbol{e}_{\mathrm{ini}}^t=\boldsymbol{\gamma}_j-\boldsymbol{s}_{t,j} \tag{17}$$

3.4 Overall objective function

In our algorithm, the state vector $\boldsymbol{X}$ contains the position, velocity, attitude, accelerometer bias, gyroscope bias, receiver clock error, and reliability vectors.

$$\boldsymbol{X}=(\boldsymbol{x}_{\mathrm{veh}},\boldsymbol{s},\boldsymbol{x}_{\mathrm{ine}}) \tag{18}$$

The least squares solution of factor graph with nodes and edges described above can be formulated as

$$\begin{aligned}\hat{\boldsymbol{X}}=&\arg\min_{\boldsymbol{X}}\sum_{t,j}\|\boldsymbol{e}_{\mathrm{vel}}^t\|_{\boldsymbol{\Omega}_{\mathrm{vel}}^t}^2+\|\boldsymbol{e}_{\mathrm{ins}}^t\|_{\boldsymbol{\Omega}_{\mathrm{ins}}^t}^2+\\&\|\boldsymbol{e}_{\mathrm{GNSS}}^t\|_{\boldsymbol{\Omega}_{\mathrm{pr}}^t}^2+\|\boldsymbol{e}_{\mathrm{rel}}^t\|_{\boldsymbol{\Omega}_{\mathrm{rel}}^t}^2+\|\boldsymbol{e}_{\mathrm{ini}}^t\|_{\boldsymbol{\Omega}_{\mathrm{ini}}^t}^2\end{aligned} \tag{19}$$

where $\boldsymbol{\Omega}_{\mathrm{vel}}^t$, $\boldsymbol{\Omega}_{\mathrm{in}}^t$, $\boldsymbol{\Omega}_{\mathrm{pr}}^t$, $\boldsymbol{\Omega}_{\mathrm{rel}}^t$, and $\boldsymbol{\Omega}_{\mathrm{ini}}^t$ are the information matrixes associated with the error functions at time t. The goal of localization issue is to find the optimal state variables that guarantee the minimization of the above error function.

4 Solution of the Incremental Optimization Problem

To solve the least squares problem as shown in Eq. (5), we need a good initial value $\hat{\boldsymbol{x}}$. We then calculate its first-order Taylor expansion, linearize the problem, use Gauss-Newton or LM algorithm to find the descent direction, and iterate the updated procedure until we find a numerical solution. $\boldsymbol{J}_t$ is then used to present the Jacobian matrix of the error function.

$$\boldsymbol{J}_t=\left.\frac{\partial\boldsymbol{e}_{ij}(\cdot)}{\partial\boldsymbol{x}}\right|_{\hat{\boldsymbol{x}}} \tag{20a}$$

$$\delta\boldsymbol{x}=\left(\boldsymbol{J}_t^{\mathrm{T}}\boldsymbol{\Omega}_{i,j}^{-1}\boldsymbol{J}_t\right)^{-1}\boldsymbol{J}_t^{\mathrm{T}}\boldsymbol{\Omega}_{i,j}^{-1}\boldsymbol{e}_{ij}(\hat{\boldsymbol{x}}) \tag{20b}$$

At each iteration, the error function is linearized on current $\hat{\boldsymbol{x}}$ over the entire trajectory, thereby showing better astringency than the EKF. Given the sparsity of the Jacobian matrix, Cholesky decomposition can be calculated in real-time. The back-end process has several mature algorithms, e.g., g^{2}o[22], iSAM2[14], which can be used directly.

5 Results

This section presents the evaluation of the proposed method. We use datasets with artificial noise to demonstrate the validity of our algorithm. The ground truth trajectory is created by simulating a moving vehicle with two external sensors. The GNSS measurements are generated at 1 Hz with the biases containing atmosphere delay, receiver clock offset, and signal-in-space error. We use the Zenith model[17] to calculate atmosphere delay and a zero-mean Gaussian noise with a standard deviation of 6 m to describe the signal-in-space error. For the INS

measurements, they are generated at 50 Hz and corrupted with constant bias and zero-mean Gaussian noise in each axis. Equations (8) and (9) show the accelerometer and gyro error models. Here we use $\tilde{\boldsymbol{y}}_a$ and $\tilde{\boldsymbol{y}}_g$ to present the static component of biases, and $\boldsymbol{\sigma}_a$ as well as $\boldsymbol{\sigma}_g$ to present the root Power Spectral Density (PSD) of inertial sensor noise. In the simulation, the relevant parameters are set as follows:

$$\tilde{\boldsymbol{y}}_a = \left(\tilde{y}_a^{\text{North}}, \tilde{y}_a^{\text{East}}, \tilde{y}_a^{\text{Down}}\right) = (9, -12, 8)\,\text{mg};$$
$$\tilde{\boldsymbol{y}}_g = \left(\tilde{y}_g^{\text{North}}, \tilde{y}_g^{\text{East}}, \tilde{y}_g^{\text{Down}}\right) = (-180, 240, -160)\ \text{deg/h};$$
$$\boldsymbol{\sigma}_a = 100 \cdot \mathbf{1}_{1\times 3}\ \mu\text{g} \cdot \text{Hz}^{-1/2};$$
$$\boldsymbol{\sigma}_g = 0.5 \cdot \mathbf{1}_{1\times 3}\ \text{deg} \cdot \text{h}^{-1/2}.$$

After generating a 2-min data fragment, we added some specific errors to the original GNSS measurements. During the entire process, seven satellites can be observed, and the number of visible satellites is adequate for positioning. The entire trajectory is divided into five sections:

- From the beginning to 20 s, only continuous noise is added to the pseudo-range measurements of two designated satellites. This section aims to test the performance when more than two satellites return faulty signals at the same time.
- From 21 s to 40 s, only continuous noise is added to the pseudo-range rate measurements of two designated satellites. This section aims to test the performance when pseudo-range rate measurements are contaminated.
- From 41 s to 60 s, two satellites are selected and continuous noise is added to their pseudo-range measurements. Meanwhile, another two satellites are selected, and continuous noise is added to their pseudo-range rate measurements. This section aims to test the performance when both the pseudo-range and pseudo-range rate of a same satellite are contaminated.
- From 61 s to 90 s, noise is added to several raw pseudo-range and pseudo-range rate measurements randomly. This section aims to test the performance when a satellite changes available state suddenly.
- From 91 s to the end, we add errors that build up gradually to the pseudo-range measurements of three designated satellites. This section aims to test the performance when innovation filters may fail theoretically.

The standard deviation of artificial error is three times the signal in space error, and the simulation produces 192 pseudo-range errors. Finally, 118 pseudo-range rate errors are obtained. The results of simple EKF, EKF with innovation filtering, and graph optimization are shown in Figs. 3–5.

The comparison of the three positioning algorithms reveals that the simple EKF is most sensitive to disturbances. Innovation filtering can exclude the measurement whose normalized innovation exceeds the fixed threshold. From 90 s to the end, the innovation filter

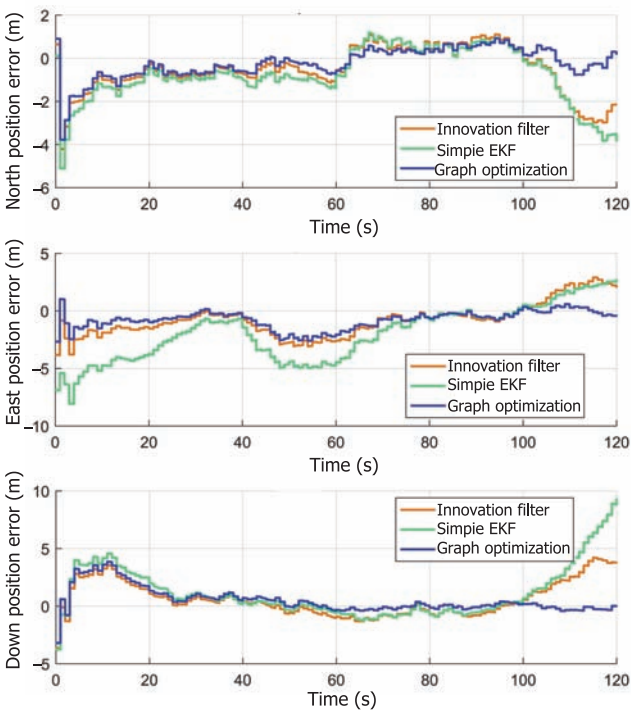

Fig. 3 Positioning errors of NED coordinate.

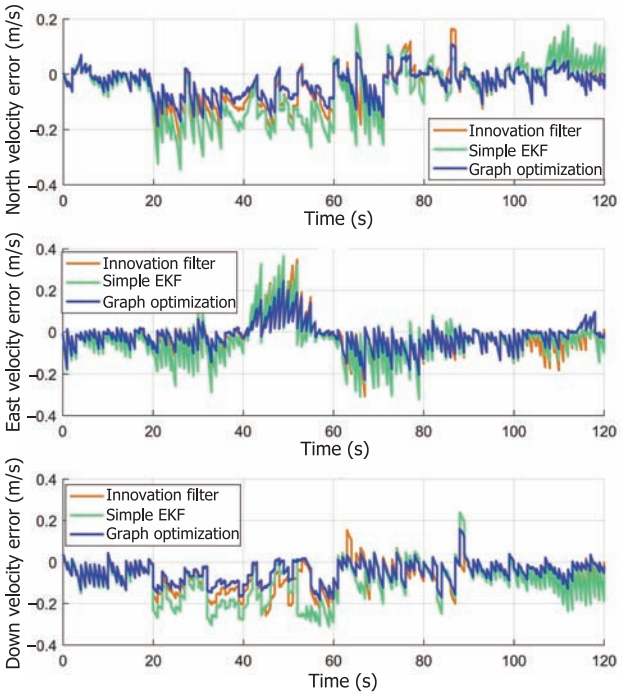

Fig. 4 Velocity errors of NED coordinate.

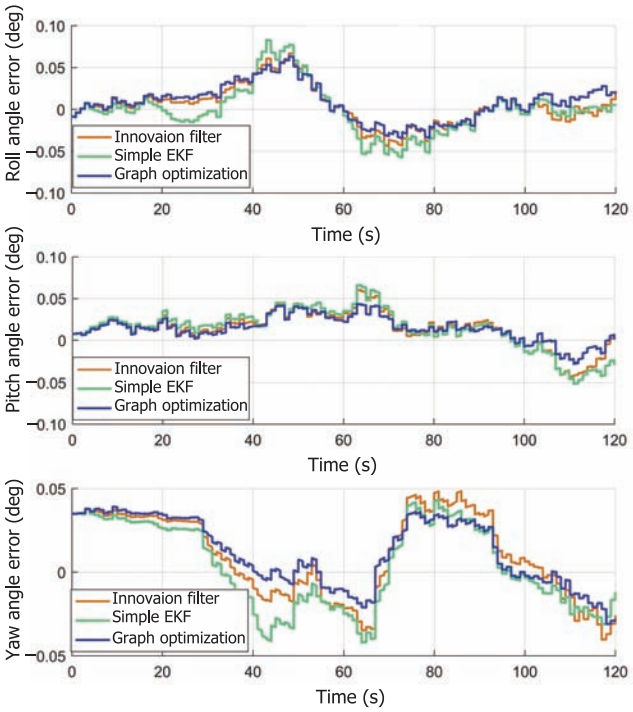

Fig. 5 Attitude errors of NED coordinate.

performs poorly when the noise increases gradually and stays constant. Moreover, the fixed threshold is also one of its defects. Compared with the adaptive threshold, the former is less flexible and may fail when most of the faults are right below the fixed threshold. The graph optimization method shows ideal performance in the last 30 s of the experiment because the previous positioning will make the current solution difficult to deviate from the true trajectory. Even when the noise is increasing slowly, the corrupted measurements can be identified through the pseudorange residuals.

We accomplish back-end optimization by using g^{2}o framework[22]. After the optimization, the comparison of the reliability factors $s^1_{t,j}$ and pseudo-range residuals is shown in Fig. 6, whereas the comparison of $s^2_{t,j}$ and pseudo-range rate residuals is shown in Fig. 7. Evidently, the reliability factor sharply decreases when the faulty GNSS measurement appears. By setting a proper threshold or choosing a clustering algorithm, our method can identify the satellite faults effectively. In our simulation, the method achieves a detection rate of 86.79%, and some artificial noises may not be large enough to detect.

All experiments were conducted on a laptop computer with Intel Core i7-4700M, 8 GB RAM. The proposed graph optimization algorithm takes 318 ms to process a 10 s data fragment. With the help of the sliding window, a compromise method can be found, which may satisfy the

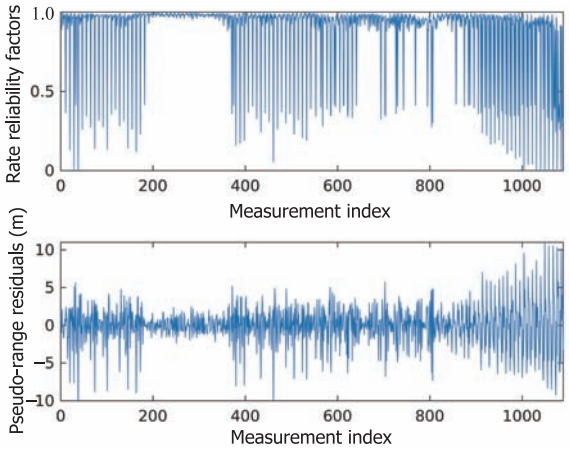

Fig. 6 Comparison of the reliability factors and pseudo-range residuals.

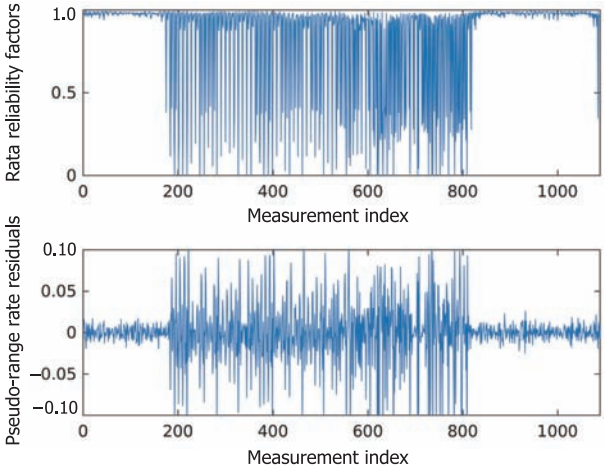

Fig. 7 Comparison of the reliability factors and pseudo-range rate residuals.

real-time performance and provide redundant data for consistency assessment.

6 Conclusion

In this paper, the GNSS/INS integrated navigation system is implemented by the optimization method instead of the most widely used filtering method. Batch optimization brings a large amount of computation because of iterations over the entire trajectory. We model the localization process as a factor graph, so the sparsity of the observation model can be exploited to reduce the computational complexity of Cholesky decomposition and satisfy the real-time constraint. The new algorithm takes advantage of previous GNSS measurements to supply redundant information, as well as INS measurements for motion constraints. Data redundancy is conducive to outlier

rejection. By introducing a reliability factor to construct a new error function, we implement satellite fault detection under the aid of INS.

The simulation results using datasets with artificial noise demonstrate that reliability factor can indicate the satellite faults effectively. Compared with the innovation filter, our algorithm performs better when the measurement errors are gradually increasing. The novel positioning algorithm can meet the requirements of both accuracy and integrity in urban vehicle navigation.

Our future work aims to test the proposed method on real-world datasets and apply the carrier phase differential technique (real-time kinematic) instead of pseudo-range positioning. Thus, some new state variables, such as integer ambiguity, will be considered when solving the optimization problem. Fortunately, new factors can be incorporated into the original graph structure in a convenient way. However, mixed integer estimation will complicate the formulation of the positioning problem.

References

[1] Y. C. Lee, Receiver autonomous integrity monitoring availability for GPS augmented with barometric altimeter aiding and clock coasting, *Global Positioning System: Theory and Applications*, vol. 2, pp. 221–242, 1996.

[2] S. S. Jan, D. Gebre-Egziabher, T. Walter, and P. Enge, Improving GPS-based landing system performance using an empirical barometric altimeter confidence bound, *IEEE Transactions on Aerospace and Electronic Systems*, vol. 44, no. 1, pp. 127–146, 2008.

[3] U. I. Bhatti, W. Y. Ochieng, and S. Feng, Integrity of an integrated GPS/INS system in the presence of slowly growing errors. Part I: A critical review, *GPS Solutions*, vol. 11, no. 3, pp. 173–181, 2007.

[4] D. Dusha and L. Mejias, Error analysis and attitude observability of a monocular GPS/visual odometry integrated navigation filter, *The International Journal of Robotics Research*, vol. 31, no. 6, pp. 714–737, 2012.

[5] A. S. Abbott and W. E. Lillo, Global positioning systems and inertial measuring unit ultratight coupling method, U.S. Patent 6516021, Feb. 2003.

[6] G. Falco, M. Pini, and G. Marucco, Loose and tight GNSS/INS integrations: Comparison of performance assessed in real urban scenarios, *Sensors*, vol. 17, no. 2, 2017.

[7] J. Farrell, *Aided Navigation: GPS with High Rate Sensors*, 1st ed. New York, NY, USA: McGraw-Hill, Inc., 2008.

[8] J. L. Crassidis, Sigma-point Kalman filtering for integrated GPS and inertial navigation, *IEEE Transactions on Aerospace and Electronic Systems*, vol. 42, no. 2, pp. 750–756, 2006.

[9] T. D. Barfoot, *State Estimation for Robotics*. Cambridge University Press, 2017.

[10] G. Sibley, L. Matthies, and G. Sukhatme, A sliding window filter for incremental SLAM, in *Unifying Perspectives in Computational and Robot Vision*, D. Kragic and V. Kyrki, eds. Springer, 2008, pp. 103–112.

[11] V. Indelman, S. Williams, M. Kaess, and F. Dellaert, Factor graph based incremental smoothing in inertial navigation systems, in *2012 15th International Conference on Information Fusion*, 2012, pp. 2154–2161.

[12] F. R. Kschischang, B. J. Frey, and H. A. Loeliger, Factor graphs and the sum-product algorithm, *IEEE Transactions on Information Theory*, vol. 47, no. 2, pp. 498–519, 2001.

[13] J. Folkesson and H. Christensen, Graphical SLAM—A self-correcting map, in *Proc. IEEE Intl. Conf. Robot. Autom. (ICRA)*, 2004, vol. 1, pp. 383–390.

[14] M. Kaess, H. Johannsson, R. Roberts, V. Ila, J. J. Leonard, and F. Dellaert, iSAM2: Incremental smoothing and mapping using the Bayes tree, *The International Journal of Robotics Research*, vol. 31, no. 2, pp. 216–235, 2012.

[15] B. W. Parkinson and P. Axelrad, Autonomous GPS integrity monitoring using the pseudorange residual, *Navigation*, vol. 35, no. 2, pp. 255–274, 1988.

[16] M. A. Sturza, Navigation system integrity monitoring using redundant measurements, *Navigation*, vol. 35, no. 4, pp. 483–501, 1988.

[17] P. D. Groves, *Principles of GNSS, Inertial, and Multisensor Integrated Navigation Systems*. Norwood, MA, USA: Artech House, 2008.

[18] N. Sünderhauf, M. Obst, G. Wanielik, and P. Protzel, Multipath mitigation in GNSS-based localization using robust optimization, in *2012 IEEE Intelligent Vehicles Symposium*, 2012, pp. 784–789.

[19] N. Sünderhauf, M. Obst, S. Lange, G. Wanielik, and P. Protzel, Switchable constraints and incremental smoothing for online mitigation of non-line-of-sight and multipath effects, in *2013 IEEE Intelligent Vehicles Symposium (IV)*, 2013, pp. 262–268.

[20] N. Sünderhauf and P. Protzel, Switchable constraints for robust pose graph SLAM, in *2012 IEEE/RSJ International Conference on Intelligent Robots and Systems*, 2012, pp. 1879–1884.

[21] E. Kaplan and C. Hegarty, *Understanding GPS: Principles and Applications*. Norwood, MA, USA: Artech house, 2005.

[22] R. Kmmerle, G. Grisetti, H. Strasdat, K. Konolige, and W. Burgard, g^2o: A general framework for graph optimization, in *2011 IEEE International Conference on Robotics and Automation*, 2011, pp. 3607–3613.

Wei Li received the BS degree from Tsinghua University, China, in 2014. She is currently pursuing the PhD degree in electronic engineering at Tsinghua University. Her major research focuses on robust and accurate algorithms for GNSS/INS integrated navigation.

Xiaowei Cui is an associate professor at the Department of Electronic Engineering, Tsinghua University, Beijing, China. He is a member of the Expert Group of China BeiDou Navigation Satellite System. His research interests include robust GNSS signal processing, multipath mitigation techniques, and high-precision positioning. He obtained both the BS and PhD degrees in electronic engineering from Tsinghua University, in 1999 and 2005, respectively.

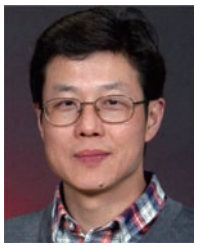

Mingquan Lu is a professor of the Department of Electronic Engineering, Tsinghua University, Beijing, China. He is the director of Tsinghua Position, Navigation, and Timing Center, and a member of the Expert Group of China BeiDou Navigation Satellite System. His current research interests include GNSS signal design and analysis, GNSS signal processing and receiver development, and GNSS system modeling and simulation. He received the ME and PhD degrees in electronic engineering from University of Electronic Science and Technology, Chengdu, China, in 1993 and 1999, respectively.